

Title No. 115-S27

Experimental Behavior of Glass Fiber-Reinforced Polymer-Reinforced Concrete Columns under Lateral Cyclic Load

by Mohammed G. Elshamandy, Ahmed Sabry Farghaly, and Brahim Benmokrane

The present study addresses the feasibility of reinforced concrete columns totally reinforced with glass fiber-reinforced polymer (GFRP) bars achieving the drift requirements specified in various codes. Eleven full-scale concrete columns—two reinforced with steel bars (as reference specimen) and nine totally reinforced with GFRP bars—were constructed and tested to failure under quasi-static reversed cyclic lateral loading and simultaneously subjected to constant compression axial load. The reported test results clearly show that properly designed and detailed GFRP-reinforced concrete columns could reach high deformation levels with no strength degradation. The results also show that the achieved drift satisfies the limitation in most building codes. Acceptable levels of energy dissipation and ductility parameters, compared to the steel-reinforced columns, were observed. The promising results can provide impetus for constructing concrete columns reinforced with GFRP and constitute a step toward using GFRP reinforcement in lateral-resisting systems such as reinforced concrete frames.

Keywords: concrete columns; ductility parameters; energy dissipation; glass fiber-reinforced polymer (GFRP) bars; hysteretic response.

INTRODUCTION

The use of fiber-reinforced polymers (FRPs) as a construction material has increased in recent years, primarily because of their noncorrodible nature and high tensile strength. FRP bars have high strength-to-weight ratios, relatively high fatigue strength, high electromagnetic transparency, and low relaxation characteristics in comparison to steel reinforcement (ACI Committee 440 2007; *fib* Task Group 9.3 2007), delivering an acceptable level of strength and deformation and offering a structurally sound alternative in most applications such as beams and bridge deck slabs (Kassem et al. 2011; Bakis et al. 2002; El-Salakawy et al. 2005).

Columns figure among the structural elements that can be exposed to severe environmental conditions. The main application of FRPs in columns has been as glass and carbon sheets externally bonded to concrete for confinement and rehabilitation purposes. Studies conducted by Alsayed et al. (1999), Choo et al. (2006), De Luca et al. (2010), Tobbi et al. (2012), Zadeh and Nanni (2013), and Afifi et al. (2014) showed the feasibility of using FRP bars exclusively to internally reinforce columns subjected to concentric compression axial load. In lateral-resisting systems such as frames—columns are part of such systems—it is important to ensure adequate stiffness and acceptable levels of dissipated energy and deformability for resisting lateral loads induced by wind or earthquakes. FRP bars show linear stress-strain behavior up to failure without any ductility, which differs from steel bars. Due to the lack of experimental data, the current ACI 440.1R (2015) design guidelines do not recommend the

use of FRP bars as longitudinal reinforcement in compression members. CSA S806 (2012), however, states that the compressive contribution of FRP longitudinal reinforcement is negligible.

Little research has been conducted on lateral-resisting concrete systems reinforced solely with FRP bars. For example, Mohamed et al. (2014) studied glass FRP (GFRP)-reinforced concrete shear walls and concluded that properly designed and detailed GFRP-reinforced shear walls could reach their flexural capacities with no strength degradation and that the failure mode could be effectively controlled. Mady et al. (2011) studied the seismic behavior of beam-column joints solely reinforced with GFRP bars and stirrups and concluded that the GFRP-reinforced joints could successfully sustain a 4.0% drift ratio without incurring significant damage.

In particular, the experimental results of laterally loaded FRP-reinforced columns (Choo et al. 2006; Sharbatdar and Saatcioglu 2009; Tavassoli et al. 2015; and Ali and El-Salakawy 2016) show a stable response and large drift ratios at failure with acceptable levels of energy dissipation, confirming the effectiveness of the FRP transverse reinforcement. This played a major role in enhancing the confinement of the concrete core, which delays concrete crushing.

The main objective of this study was to demonstrate the feasibility of using GFRP bars as longitudinal and transverse reinforcement in concrete columns subjected to combined axial and cyclic lateral loads. The objective relied on a comprehensive experimental program involving full-scale GFRP-reinforced columns with different detailing configurations, longitudinal reinforcement ratios, transverse volumetric ratios, and axial load ratio.

RESEARCH SIGNIFICANCE

Experimental research is needed to verify the applicability of concrete columns reinforced with longitudinal and transverse GFRP bars under different stress conditions, particularly under simulated seismic loads. This poses serious concerns about their feasibility in earthquake-resistant structures, in which seismic energy is expected to be dissipated by inelasticity in members. Full-scale GFRP-reinforced concrete columns were tested to investigate the behavior of these columns and assess their significance from a seismic performance perspective based on the dissipated energy and

ACI Structural Journal, V. 115, No. 2, March 2018.

MS No. S-2016-151.R1, doi: 10.14359/51700985, was received April 7, 2017, and reviewed under Institute publication policies. Copyright © 2018, American Concrete Institute. All rights reserved, including the making of copies unless permission is obtained from the copyright proprietors. Pertinent discussion including author's closure, if any, will be published ten months from this journal's date if the discussion is received within four months of the paper's print publication.

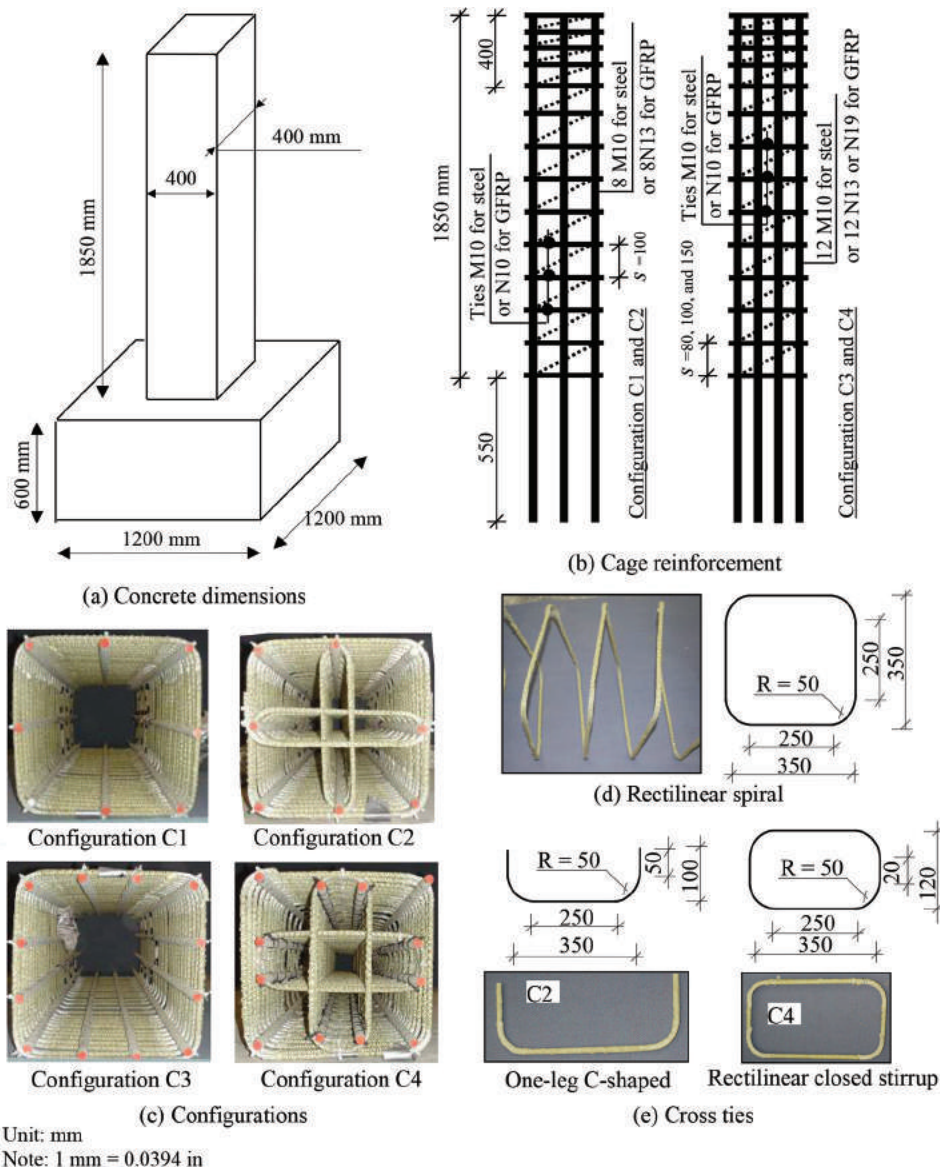


Fig. 1—Test specimen details.

ductility levels attained. This study is expected to set the path for further research to investigate the possibility of developing new applications of GFRP bars, resulting in more durable, economic, and competitive medium-rise reinforced concrete buildings in low-to-moderate seismic zones.

EXPERIMENTAL PROGRAM

Test specimen design

The steel-reinforced columns were designed and analyzed according to the recommendations and limitations of CSA A23.3 (2014) and ACI 318 (2014), while CSA S806 (2012) was used for GFRP-reinforced columns. The nominal moments were calculated based on plane sectional analysis, taking into account the effect of applied axial load through the moment-axial load interaction diagram for the adopted axial load ratio. To satisfy the shear-capacity requirements for the specimens, transverse reinforcement (rectilinear spirals and cross ties) was provided at the maximum allowed spacing—namely, the least of: 1) 16 times the diameter of the smallest longitudinal bars; 2) 48 times the minimum cross-sectional diameter of the GFRP tie; 3) the least dimen-

sion of the compression member; or 4) 300 mm (11.8 in.). This was done for the stability of the longitudinal bars.

Description of test specimens

The experimental program consisted of 11 reinforced square concrete columns (two of them were steel-reinforced and the other nine were GFRP-reinforced) measuring 400 x 400 x 1850 mm (15.7 x 15.7 x 72.8 in.) connected to a massive stub (1200 x 1200 x 600 mm [47.2 x 47.2 x 23.6 in.]) and cast vertically. The transverse load was applied at top of the specimen 1.65 m (65 in.) from the base of the column with a displacement-controlled hydraulic actuator. The specimens represent a column 3.7 m (145.6 in.) in height in a typical building with the assumed point of contraflexure located at column midheight. Figure 1 shows the concrete dimensions and reinforcement details.

The main variables investigated were: 1) GFRP reinforcement configuration; 2) axial load level; 3) spacing and amount of the GFRP transverse reinforcement; and 4) the GFRP longitudinal reinforcement ratio. Table 1 lists the aforementioned variables. Figure 1(b) shows the GFRP cage

Table 1—Test specimen details

Specimen	f'_c	ρ_l , %	Transverse reinforcement				s	$P/f'_c A_g$	EA			
			ρ_{vs} , %	$A_{sh\ act}$	$A_{sh\ req}$ for drift							
					>2.5%	>4%						
ST8N10-C1-100	44	0.35	0.25	—	—	—	0.2	113				
ST12N10-C4-100	34	0.53	0.5	—	—	—		170				
G8N13-C1-100	37	0.63	0.36	142.6	238.9	382.2		100	71			
G8N13-C2-100	37		0.53	213.9	168.9	270.2						
G12N13-C3-100	39	0.95	0.36	142.6	251.8	402.8			150	0.2		
G12N13-C4-100	39		0.71	285.2	145.4	232.6					80	
G12N13-C4-100-30	32				178.9	286.3						0.3
G12N13-C4-100-40	33				246.0	393.6						0.4
G12N13-C4-150	41				0.48	280.8						449.2
G12N13-C4-80	41		0.89	109.4	175.0	80					0.2	
G12N19-C4-100	43		2.14	0.71	160.3	256.5	100				207	

Notes: f'_c is concrete compressive strength (MPa); ρ_l is longitudinal reinforcement ratio; ρ_{vs} is transverse reinforcement ratio; $A_{sh\ act}$ is actual provided transverse reinforcement (mm²); $A_{sh\ req}$ is required transverse reinforcement according to Eq. (6) to achieve either 2.5% or 4% drift (mm²); s is spacing of transverse reinforcement (mm); $P/f'_c A_g$ is axial load level; EA is axial stiffness; E is longitudinal bar modulus of elasticity; A is longitudinal bar area; 1 mm² = 0.00155 in.²; 1 MPa = 145 psi; 1 kN = 0.225 kip.

reinforcement of the test specimens. The axial load ratio (ALR) is defined as the index $P/f'_c A_g$, where P is the constant axially applied compression load, f'_c is the concrete compressive strength, and A_g is the gross cross-sectional area of the column. Three ALR of 20, 30, and 40% were chosen. Four different configurations were adopted to study the effect of the number of longitudinal bars and transverse crossties on the cyclic response of the laterally loaded columns (Fig. 1(c)). Figure 1(d) shows the rectilinear spiral used for the outer transverse reinforcement (stirrups). Two shapes of crossties were used as inner transverse reinforcement: one-leg C-shaped crosstie and rectilinear closed stirrup crosstie, as shown in Fig. 1(e).

The specimens are identified by reinforcement type (ST for steel and G for GFRP), number of longitudinal bars (eight and 12), longitudinal bar diameter (N10 and N8 for steel and N13 and N19 for GFRP), configuration (C1, C2, C3, and C4), and spacing (80, 100, and 150 mm [3.15, 3.94, and 5.9 in.]). In addition, the numbers 30 and 40 identify the two columns subjected to 30 and 40% ALR; the other columns were subjected to 20% ALR. It should be noted that although a spacing of 100 mm (3.94 in.) and 150 mm (5.9 in.) as well as configuration C1 and C3 do not satisfy CSA S806-12 requirements and limitations, they were chosen intentionally to meet the research goal of examining the deformation capacity of GFRP-reinforced columns. Table 1 provides the test matrix and reinforcement details of the test specimens.

Material properties

All specimens were constructed with normalweight, ready mixed concrete having a target nominal compressive strength $f'_c = 40$ MPa (5.8 ksi). Table 1 gives the actual concrete compressive strength based on the average values from tests performed on at least three 100 x 200 mm (3.94 x 7.87 in.) cylinders for each concrete batch on the column's day of testing. N10 and N8 grade 60 steel bars were used in the

Table 2—Reinforcement material properties

Bar*	d_b , mm	A_f , mm ²	E_f , GPa	f_{fu}^\dagger , MPa	ϵ_{fu} , %	
Straight bars						
GFRP	N13 (No. 4)	12.7	126.7	69.6	1392	2.00
	N19 (No. 6)	19.1	285	60.5	1125	1.82
Steel	N8 (No. 2)	8	50	200	$f_y = 400$	$\epsilon_y = 0.2$
	N10 (No. 3)	9.5	71.3	200	$f_y = 420$	$\epsilon_y = 0.2$
Bent GFRP N10 (No. 3) rectilinear spiral and crossties						
Straight	9.5	71.3	52	962	1.85	
Bent	9.5	71.3	—	500	—	

*Numbers in parentheses are manufacturer's bar designation.

†Guaranteed tensile strength is average value - 3 x standard deviation (ACI 440.1R-06).

Notes: d_b is bar nominal diameter; A_f is nominal cross-sectional area; E_f is modulus of elasticity; f_{fu} is guaranteed tensile strength; ϵ_{fu} is ultimate strain; f_y is steel yielding strength; ϵ_y is steel yielding strain; 1 mm = 0.0394 in.; 1 mm² = 0.00155 in.²; 1 MPa = 145 psi.

steel-reinforced columns as longitudinal and transverse reinforcement, respectively. The GFRP reinforcing bars in the GFRP-reinforced columns were three diameters of Grade III sand-coated bars (CSA S807 2015): N13 and N19 as longitudinal bars and N10 as transverse reinforcement (rectilinear spirals and crossties). The longitudinal tensile properties of the GFRP bars were determined by testing five specimens according to ASTM D7205 (2011), in the case of the straight bars, and test method B.5 in ACI 440.3R (2004) in the case of the bent bars. The steel-bar properties were provided by the manufacturer. Table 2 lists the material properties of the reinforcing bars.

Instrumentation

Electrical strain gauges and linear variable differential transducers (LVDTs) were used to measure strain and displacement, respectively, as shown in Fig. 2. Thirty electrical strain gauges were mounted on the longitudinal and transverse reinforcement at three different levels above the

stub. Concrete strain and curvature were calculated using three sets of LVDTs that were placed in the column faces perpendicular to the loading direction within the plastic hinge region. Four LVDTs were mounted to capture the lateral deformation at different column heights. Two additional LVDTs were used to monitor the sliding at the column-stub connection and between the stub and rigid floor.

Test setup and loading procedure

Figure 3 shows the test setup. The axial load was applied at the top of the column, where the axial stress was maintained constant throughout the test. Cyclic lateral displacements at a rate of 1.3 mm/min (0.05 in./min) were applied to the columns with a 500 kN (112.4 kip) MTS actuator mounted horizontally to a steel reaction frame. A typical

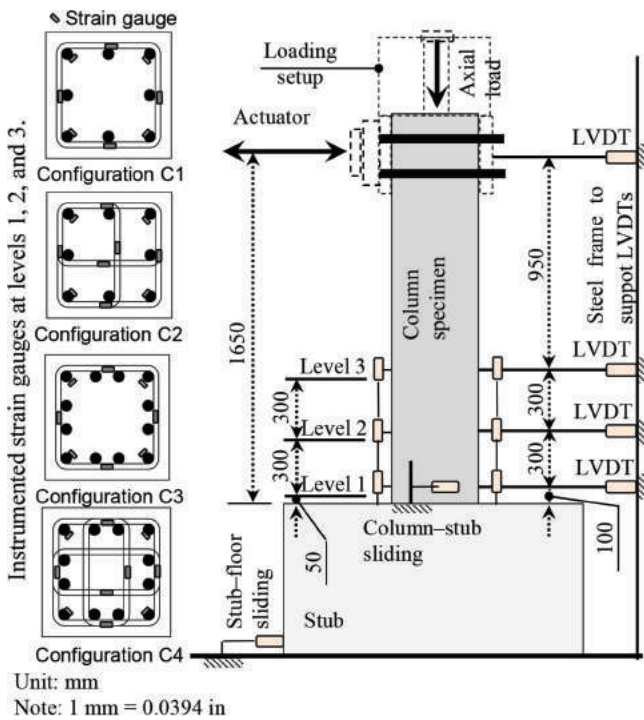


Fig. 2—Instrumentation of test specimens.

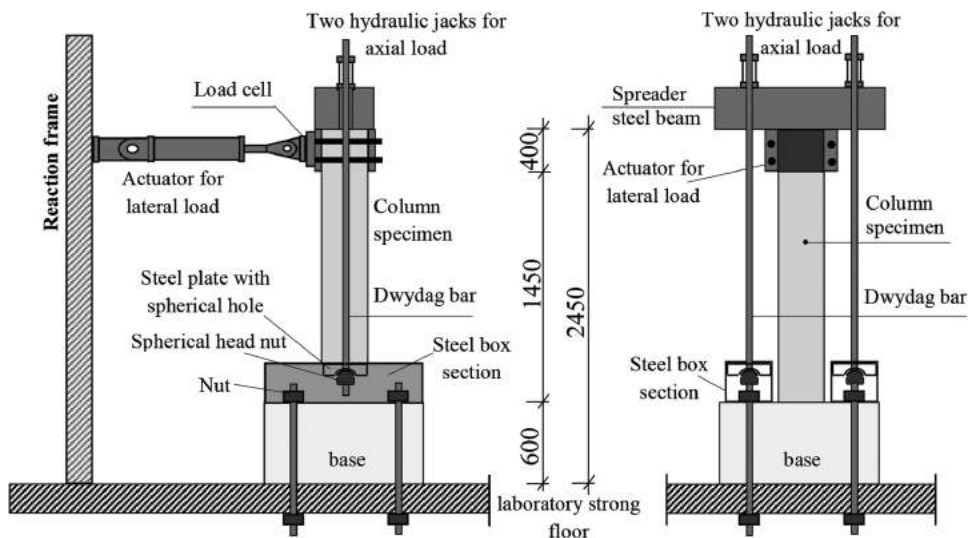


Fig. 3—Test setup.

procedure of applying quasi-static reversed cyclic loading until failure was used. Two excursions at each displacement cycle were applied with the displacement increment related to drift ratio, as shown in Fig. 4.

EXPERIMENTAL RESULTS

General behavior and response

Figure 5 provides the lateral load versus top drift for all the specimens. The second excursion loading path followed the first excursion but with less stiffness. The second excursion in each chosen lateral drift was removed for clarity. In the graphs of Fig. 5, the occurrences of special events such as the yielding of longitudinal steel bars, spalling of concrete cover, interlaminar degradation of longitudinal GFRP bars, and loss of axial load capacity due to concrete crushing are identified. The hysteretic response of each column showed reasonable symmetric lateral load-top drift relationships for loading in the positive and negative directions until concrete crushing occurred at one end.

The response was essentially linear-elastic for all columns up to development of the first crack with the GFRP-reinforced columns evidencing lower initial stiffness than the steel-reinforced ones. Thereafter, cracks started to propagate. The behavior of all the columns was dominated by a flexural response, as evidenced by the typical amount of horizontal cracking aligned with the rectilinear spirals and ties (refer to Fig. 6). Under increased displacement, horizontal cracks continued to form up to a height of approximately 60% of the column's effective height ($h_e = 1650$ mm [65 in.]) above the column base for well-confined columns, as evidenced in Fig. 6. This relates to photos for Columns ST12N10-C4-100, G12N13-C4-100-30, G12N13-C4-100-40, G12N13-C4-80, and G12N19-C4-100. As the confinement level decreased, the cracks propagated up to 50% of h_e in Columns G8N13-C2-100, G12N13-C3-100, and G12N13-C4-100 and to 40% for the columns lightly reinforced in the longitudinal or transverse direction, such as ST8N10-C1-100, G8N13-C1-100, and G12N13-C4-150. At the early loading stage, the steel bars in ST8N10-C1-100 and ST12N10-C4-100 yielded at 0.25% and 0.62% drift, respectively.

With further application of the cyclic load, vertical splitting cracks typically appeared in the columns at the compressed side of the steel- and GFRP-reinforced columns, respectively, as shown in Fig. 7(a) and 8(a). Figures 7(b) and 8(b) show the spalling of the concrete cover, which became

more significant and occurred in all the columns within a range of 1.4 to 1.9% lateral drift.

The longitudinal bars in the steel-reinforced columns buckled (Fig. 7(c)) during the displacement cycle before the concrete cover spalled, as shown in Fig. 5. Although the buckled bars straightened under tension during the reversed load cycle, degradation of the lateral resistance was more pronounced after buckling occurred in the outermost bar. With further cyclic loading, excessive steel-bar buckling was observed until the axial load was lost due to the concrete core crushing (Fig. 5 and Fig. 7(d)). On the other hand, the GFRP-reinforced columns experienced three different behaviors based on test variables as follows:

1. For lightly reinforced columns (G8N13-C1-100, G8N13-C2-100, G12N13-C3-100, and G12M13-C4-150), the strength degradation preceded concrete-cover spalling, as shown in Fig. 5.

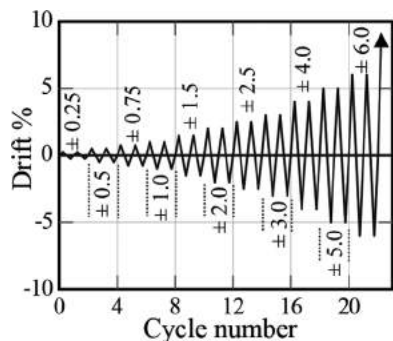


Fig. 4—Loading history.

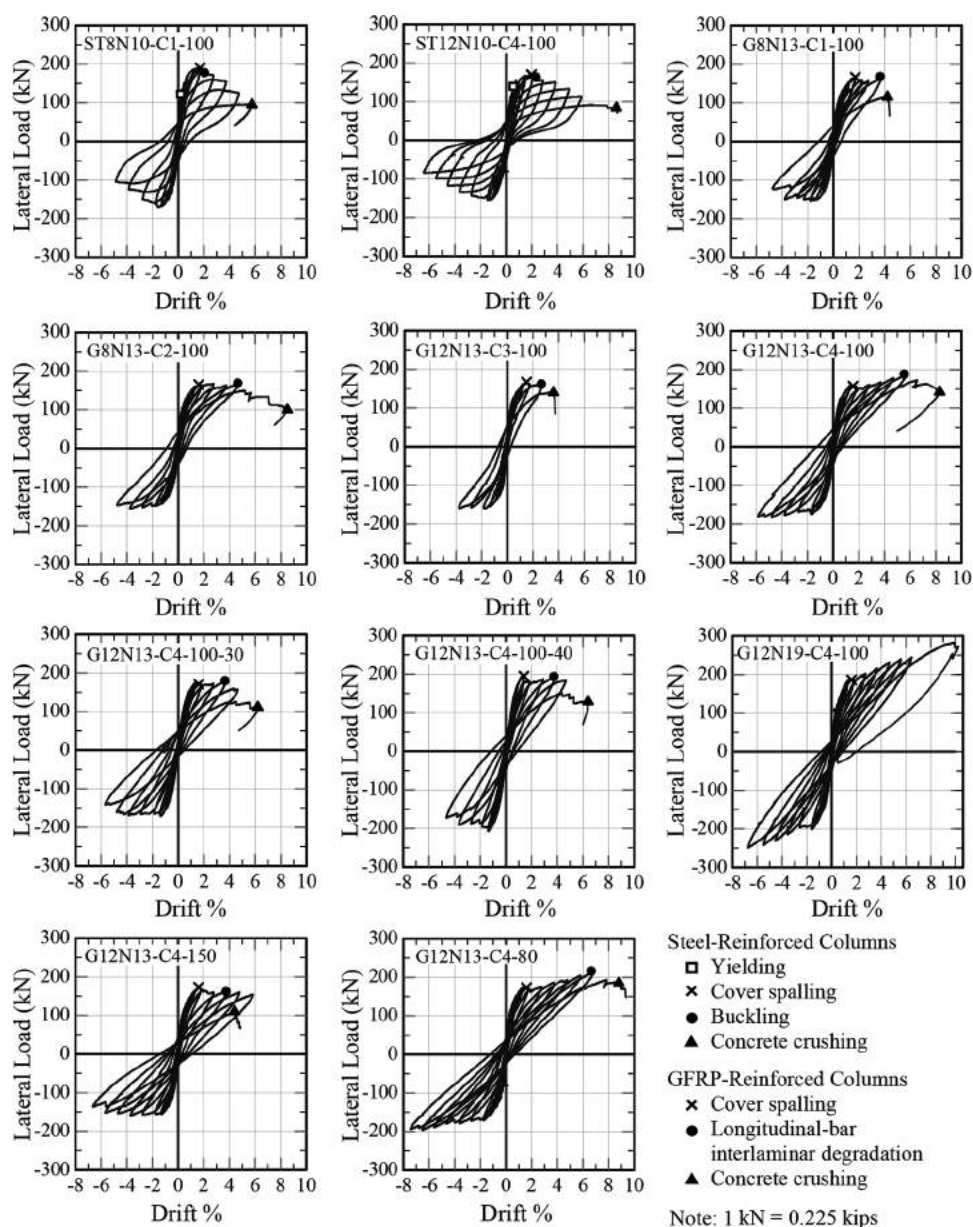


Fig. 5—Load-displacement hysteretic response.

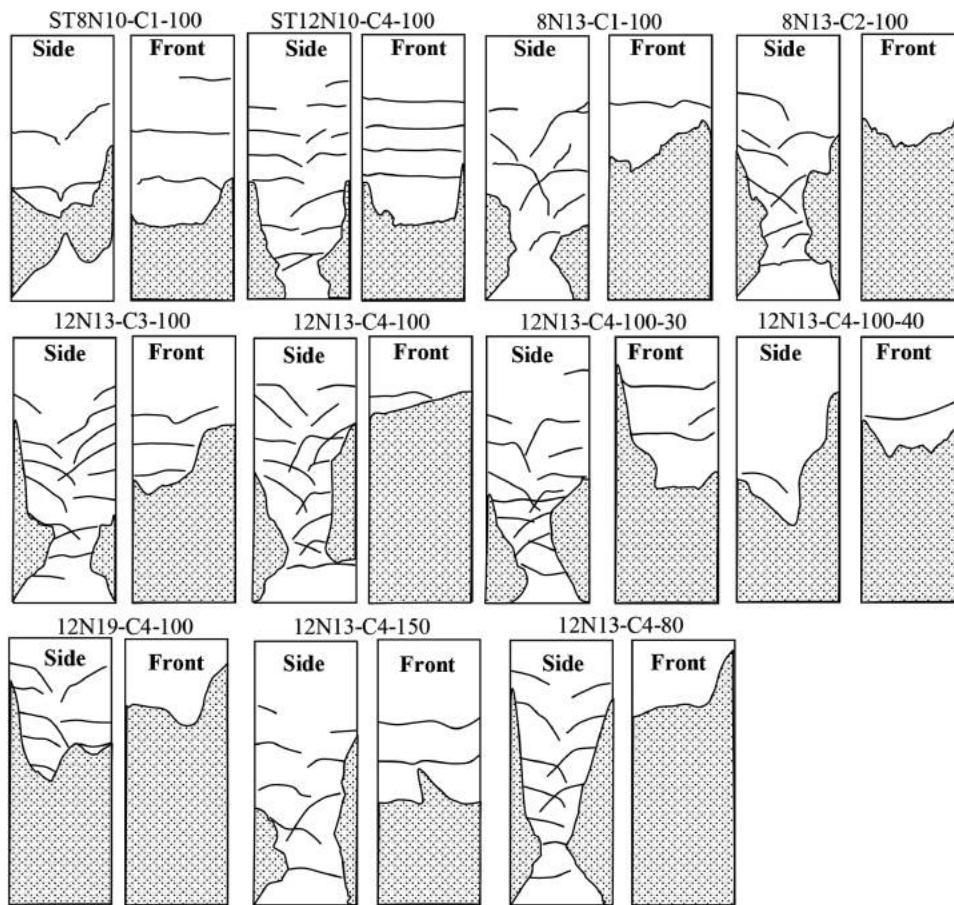


Fig. 6—Crack pattern.

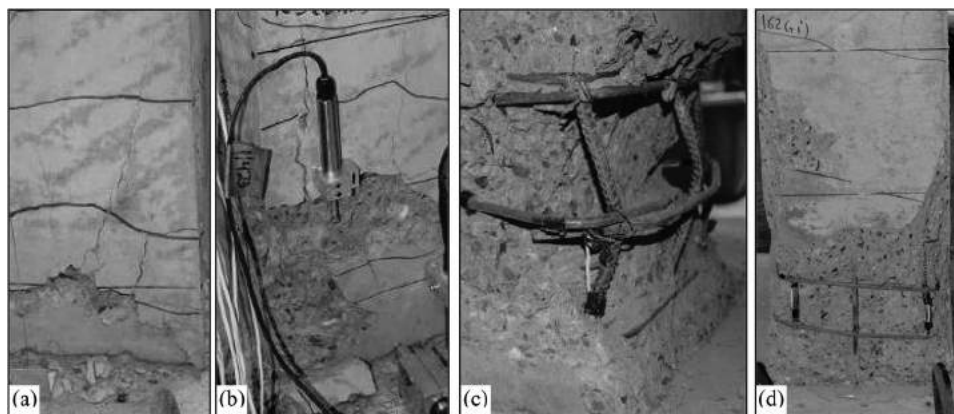


Fig. 7—Typical failure progression of steel-reinforced columns: (a) vertical splitting; (b) spalling of concrete cover; (c) buckling of longitudinal bars; and (d) concrete crushing causing failure.

2. The well-confined columns (G12N13-C4-100, G12N13-C4-80, and G12N19-C4-100) experienced a strength gain with a second peak (Fig. 5). This phenomenon has been reported in FRP-reinforced columns subjected to axial concentric compression load (Tobbi et al. 2012).

3. Increasing the axial load ratio to 30% and 40% for G12N13-C4-100-30 and G12N13-C4-100-40, respectively, controlled the strength gained in Column G12N13-C4-100, but both columns reached a plateau after the concrete cover spalled (Fig. 5).

Consequently, the GFRP-reinforced columns had responses similar to their counterpart steel-reinforced columns

with similar axial stiffness ($EA \approx 110$ MN [24,730 kip]), such as comparing ST8N10-C1-100 to G12N13-C3-100. Among the columns with higher axial stiffness ($EA \approx 190$ MN [42,710 kip]), the GFRP-reinforced column (G12N13-C4-100) performed better than its counterpart steel-reinforced column (ST12N10-C4-100). Moreover, increasing the longitudinal GFRP bars or reducing the transverse reinforcement spacing (such as in G12N19-C4-100 and G12N13-C4-80, respectively) enhanced performance as the ultimate strength and drift of the columns increased. Overall, the GFRP bars kept their integrity with no observed degradation until one or two cycles before the failure cycle.

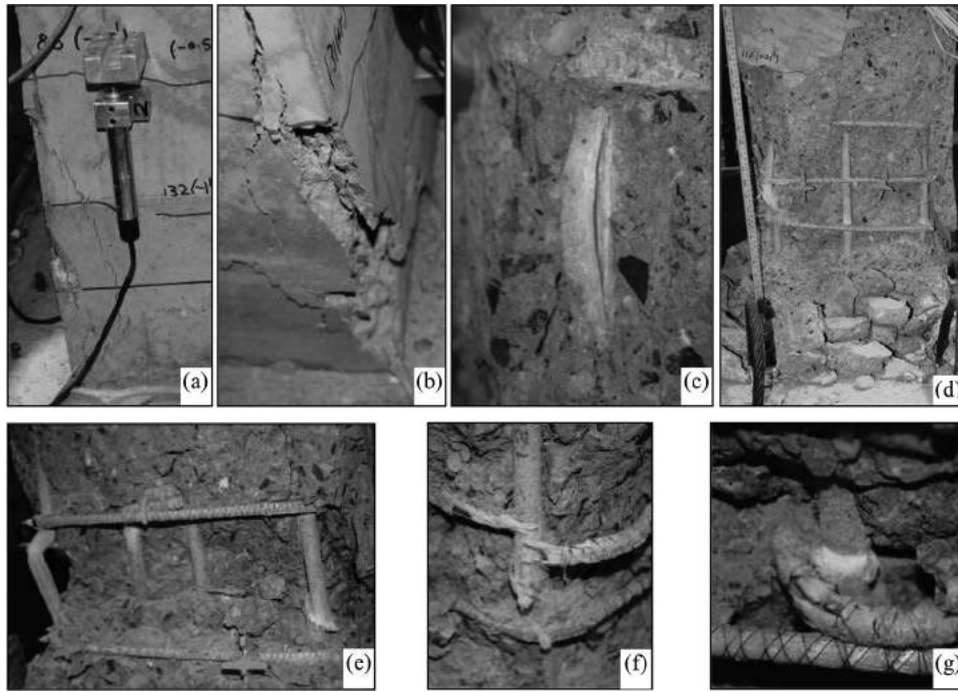


Fig. 8—Typical failure progression of GFRP-reinforced columns: (a) vertical splitting; (b) spalling of concrete cover; (c) longitudinal bar interlaminar degradation; (d) concrete crushing causing failure; (e) fracture of longitudinal GFRP bars; (f) rupture of GFRP rectilinear spirals; and (g) rupture of GFRP crossties.

Table 3—Failure progression

Specimen	Yielding		Cover spalling		Buckling		Interlaminar		Concrete crushing		P_f/P_{max}
	P , kN	δ , %	P , kN	δ , %	P , kN	δ , %	P , kN	δ , %	P , kN	δ , %	
ST8N10-C1-100	120	0.25	190	1.7	176	2.1	N/A		95	5.7	0.50
ST12N10-C4-100	137	0.62	170	1.9	161	2.4			84	8.6	0.49
G8N13-C1-100	N/A		166	1.7	N/A		166	3.7	115	4.2	0.69
G8N13-C2-100			165	1.6			167	4.7	100	8.5	0.60
G12N13-C3-100			167	1.5			160	2.7	140	3.6	0.84
G12N13-C4-100			157	1.6			186	5.6	142	8.3	0.76
G12N13-C4-100-30			171	1.6			178	3.7	111	6.2	0.62
G12N13-C4-100-40			195	1.4			192	3.8	129	6.4	0.66
G12N13-C4-150			173	1.6			160	3.8	110	4.4*	0.64
G12N13-C4-80			173	1.6			214	6.7	185	8.8	0.86
G12N19-C4-100			186	1.6			—	—	282 [†]	10.1 [†]	0.00

*G12N13-C4-150 achieved 5.6% drift; however, it failed at 4.4% drift during the following cycle.

[†]Maximum lateral load and drift attained without failure.

Note: 1 kN = 0.225 kip.

The interlaminar degradation of the compressed longitudinal GFRP bars occurred at a various drift levels with a minimum drift value of 2.7% for G12N13-C3-100 and reaching more than 3.7% drift for all the other GFRP-reinforced columns, which is higher than the 2.5% drift recommended by the *National Building Code of Canada* (NRC 2010) and CSA S806 (2012). In contrast, the steel bars lost their integrity at early drift levels of 2.1% and 2.4% in ST8N10-C1-100 and ST12N10-C4-100, respectively. Figure 8(c) shows the interlaminar degradation of the GFRP bars.

When the displacement increased, all the columns lost the axial load due to the concrete core crushing shown in Fig. 7(d) and Fig. 8(d). The failure of the GFRP-reinforced columns was associated with fracturing of compressed longitudinal GFRP bars (Fig. 8(e)) and rupture of GFRP rectilinear spirals and ties (Fig. 8(f) and (g), respectively). There was one exception: Column G12N19-C4-100 reached the limit of the loading setup at 10% lateral drift with no interlaminar degradation or failure due to the greater longitudinal bar diameter. Table 3 provides the failure progression.

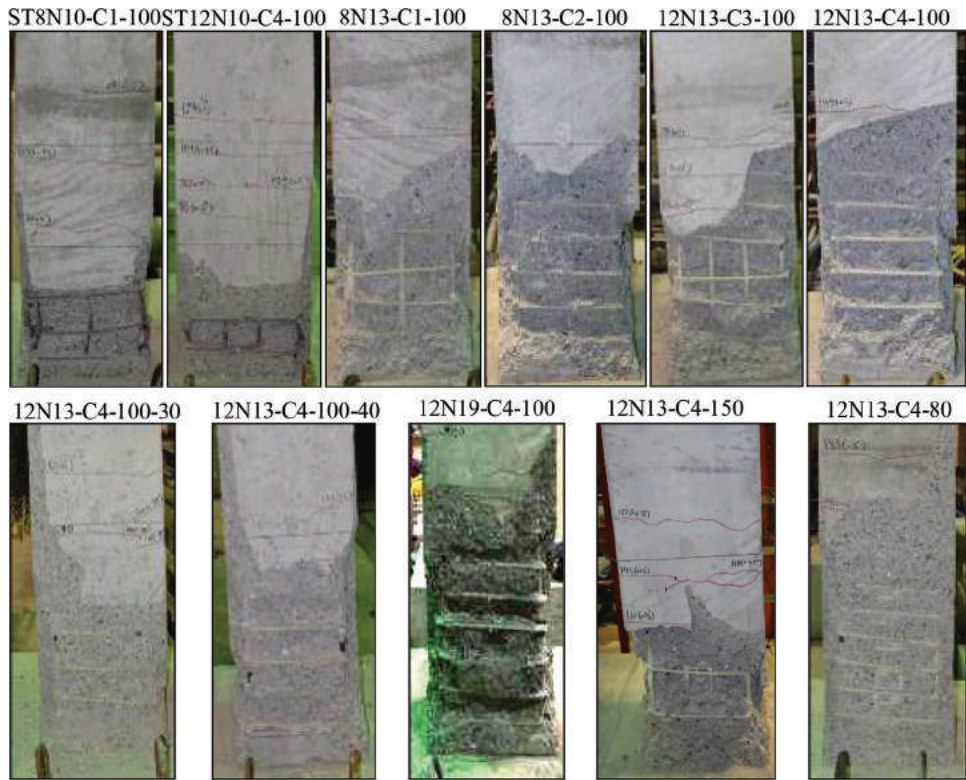


Fig. 9—Plastic hinge zone.

The photos in Fig. 9 show the plastic hinge zone after the failure of the test specimens. Generally, based on the damaged region, the smaller the level of confinement, the larger the tie spacing, and the larger the axial load ratio, the larger the column's damaged region. Figure 9 also shows that the damaged zone in all the columns started at a distance of 25 to 30 mm (1 to 1.2 in.) above the base stub. This behavior, observed in similar specimens by other researchers (Ali and El-Salakawy 2016; Sheikh and Houry 1993) has been attributed mainly to the base stub providing confinement to the column sections just above it. Therefore, the moment is calculated at 30 mm (1.2 in.) above the column-stub interface.

Ductility and energy dissipation

Ductility parameters and energy dissipation capacity are usually used to assess the seismic response of reinforced concrete members. While the ductility of long-period structures is directly related to the strength reduction factor used in many codes (CSA S806-12 and NRC [2010]) to calculate the seismic base shear, the energy-dissipation capacity can be used as a response indicator in the design of short-period structures and structures subjected to a long-duration earthquake.

Ductility parameters—The ductility index is a parameter that provides an indication of a system's capacity to deform beyond the elastic range, which is important in areas of earthquake activity where absorbing energy is of prime importance. Conventional ductility indexes are defined as the ratio of the final deformation at the ultimate state to the deformation at the first plastic behavior. Therefore, a well-defined transition point from elastic to inelastic deformation of GFRP-reinforced columns should be investigated

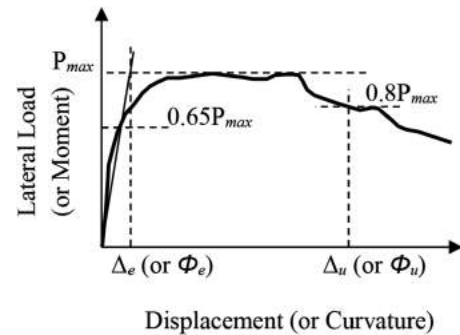


Fig. 10—Idealized curve definition.

to calculate the ductility index. Due to the lack of research concerning the ductility index, ACI 440.1R (2015) and CSA S806 (2012) design codes offer no unified method for assessing the ductility index of FRP-reinforced structures.

For the steel-reinforced columns, the elastic region ended at yield-deformation point Δ_y and the inelastic region at maximum deformation point Δ_u . For GFRP-reinforced columns, the elastic region ended at the start of concrete inelasticity—that is, concrete deterioration at the compressed end of the column—and the inelastic region at the maximum deformation point. The major difference between the steel- and GFRP-reinforced columns is the absence of yielding phenomena in the GFRP bars. For this reason, the transition point between the elastic and inelastic regions in GFRP-reinforced columns is defined herein as the virtual yield deformation point Δ_e . Accordingly, the load-displacement and the moment-curvature curves are used to identify the elastic branch of the idealized curve (Fig. 10). In the load-displacement curve, the elastic branch is secant to the real curve at 65% of the maximum lateral load P_{max} , and reaches the maximum

Table 4—Ductility parameters

Specimen	$\delta, \%$	μ_{Δ}	μ_{ϕ}	J	
				$J_{0.001}$	$J_{0.0035}$
ST8N10-C1-100	5.7	6.6	>7.1	—	—
ST12N10-C4-100	8.6	7.7	>9.0	—	—
G8N13-C1-100	4.2	5.5	>8.2	28.3	5.9
G8N13-C2-100	8.5	10.4	>12.3	41.2	10.1
G12N13-C3-100	3.6	7.8	>9.7	32.9	8.5
G12N13-C4-100	8.3	9.8	>12.5	37.6	10.0
G12N13-C4-100-30	6.2	5.6	>7.9	27.5	6.1
G12N13-C4-100-40	6.4	6.6	>8.5	34.7	6.4
G12N13-C4-150	4.4	7.1	>11.2	31.8	7.3
G12N13-C4-80	8.8	9.8	>10.9	39.5	10.9
G12N19-C4-100	>10.1	>7.5	>9.9	>33.6	>7.9

load to define the virtual yield deformation point Δ_e . Column failure is conventionally defined at the post-peak displacement Δ_u , at which point the remaining capacity of the column has dropped to 80% (Tavassoli et al. 2015) of the peak load. The moment-curvature curve is used in a similar procedure (Fig. 10).

The displacement ductility index μ_{Δ} is defined as

$$\mu_{\Delta} = \frac{\Delta_u}{\Delta_y} \text{ for steel or } \mu_{\Delta} = \frac{\Delta_u}{\Delta_e} \text{ for FRP} \quad (1)$$

and the curvature ductility index μ_{ϕ} is defined as

$$\mu_{\phi} = \frac{\phi_u}{\phi_y} \text{ for steel or } \mu_{\phi} = \frac{\phi_u}{\phi_e} \text{ for FRP} \quad (2)$$

A concept based on deformability rather than ductility was proposed to ensure adequate deformation of FRP-reinforced structures before failing, based on the work reported by Jaeger et al. (1995). The concept was developed for FRP-reinforced beams and slabs. A combination of strength and deformability was incorporated into the deformability factor J , which can be regarded as the ratio of two energy quantities: one associated with the ultimate limit-state condition, and the other to the condition when the concrete at the extreme compression fiber reaches its proportional limit. The deformability factor is expressed as follows (Jaeger et al. 1995)

$$J = \frac{M_u \phi_u}{M_c \phi_c} \quad (3)$$

where M and ϕ are the moment and curvature at service or ultimate, denoted by the subscripts c and u , respectively. The Canadian Highway Bridge Design Code (CHBDC) includes an overall performance factor for FRP-reinforced beams and slabs (CSA S6-14 2014) that combines the strength and deformability given by Eq. (3), with the service condition, taken as the point when the maximum concrete compressive strain reaches 0.001.

For the GFRP-reinforced columns, J was calculated and resulted in unreliably high values (referred as $J_{0.001}$ in

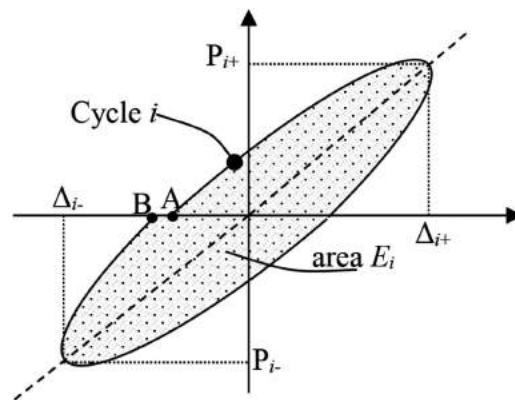


Fig. 11—Definition of energy dissipation.

Table 4). As the moment and curvature were determined at a concrete compressive strain of 0.001 (the recommended value for FRP-reinforced beams and slabs according to CSA S6-14 and CSA S806-12), high values of $J_{0.001}$ were reached due to well-confined concrete, which allowed the concrete compressive strain to reach more than 0.008 at ultimate. Therefore, the deformability factor J was recalculated for moment and curvature values corresponding to a concrete compressive strain of 0.0035 ($J_{0.0035}$). Table 4 lists the original $J_{0.001}$ and modified $J_{0.0035}$ deformability factor resulting in a large difference between the two procedures due to the difference in the values of moments and curvatures corresponding to concrete compressive strains of 0.001 and 0.0035. The calculated $J_{0.0035}$ showed reliable values in comparison to the other procedures (Mohamed et al. 2015).

The main drawback of using the ductility parameters is the lack of consensus in the research community on a definition of the elastic-plastic transition point in FRP-reinforced concrete members. The maximum interstory drift δ_u is simpler to use and is defined based on the measured displacement at failure as $\delta_u = \Delta_u/h_e$ (Table 4).

The calculated ductility indexes listed in Table 4— μ_{Δ} , μ_{ϕ} , J , and δ_u for the GFRP-reinforced columns—showed consistency in representing the effect of each studied parameter on the ductility indexes. The displacement ductility μ_{Δ} and deformability factor $J_{0.0035}$ showed reasonable predicted ductility indexes while the curvature ductility μ_{ϕ} showed higher estimation of the columns' ductility and $J_{0.001}$ might be considered inappropriate due to the confinement level profound in the columns.

Energy dissipation—Energy dissipation is recognized as an important parameter with respect to a structure's seismic performance. Energy dissipation is defined for a cycle i by the shaded area in Fig. 11 or mathematically as follows

$$E_i = \int_A^B F du \quad (4)$$

The accumulated energy dissipation E_{acc} during the test until failure in each cycle is defined as

$$E_{i acc} = \sum_1^i E_i \quad (5)$$

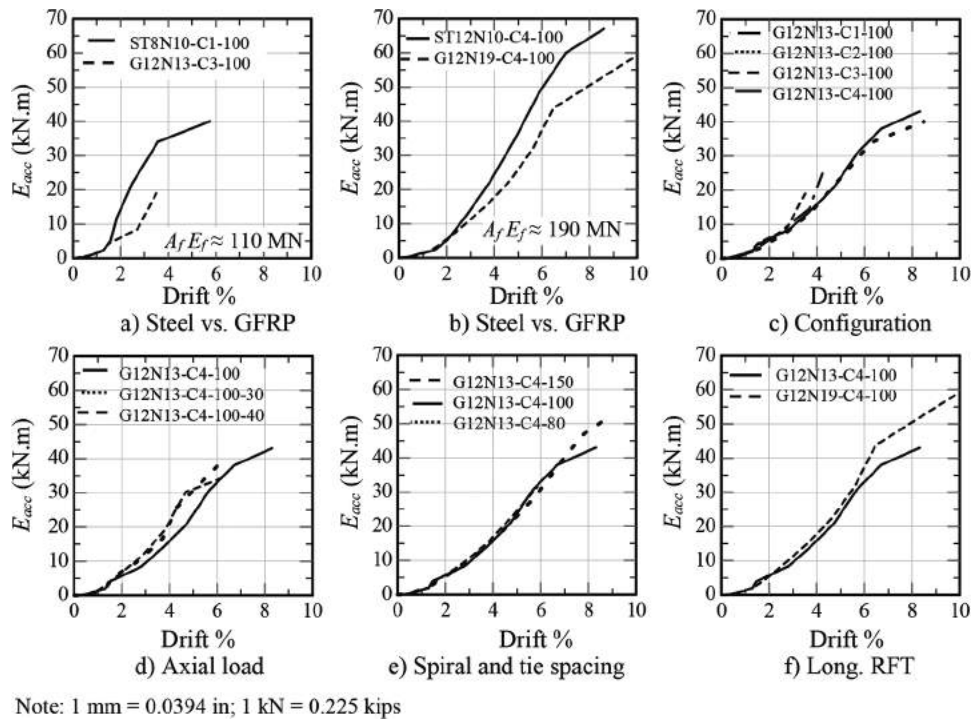


Fig. 12—Cumulated energy dissipation. (Note: 1 kN.m = 0.738 kip.ft.)

Figure 12 shows the calculated E_{acc} in each cycle for the tested columns. For drifts lower than 1%, E_{acc} was quite small. For larger drifts, however, an increase in the dissipated energy with respect to an increase in drift level can be observed. Close to the final stage, a slight decrease in the tendency rate was observed.

The dissipated energy of the steel- and GFRP-reinforced columns can be compared for lower axial stiffness (≈ 110 MN [24,730 kip]) and higher axial stiffness (≈ 190 MN [42,710 kip]). Columns ST8N10-C1-100 and G13-C3-100 (Fig. 12(a)), with lower axial stiffness, exhibited similar dissipated energy up to 1.7% drift, which was prior to the buckling of the steel bars. Thereafter, with increased drift, however, ST8N10-C1-100 achieved higher E_{acc} compared to G12N13-C3-100. At 2.5%—corresponding to moderate ductility according to CSA S806-12—the E_{acc} of ST8N10-C1-100 was almost the double that of G12N13-C3-100, which was expected due to the excessive longitudinal steel-bar buckling occurring before 2% drift led to early degradation of the column, resulting in significant dissipated energy. In contrast, G12N13-C3-100 kept its integrity until a higher drift level (2.7%, corresponding to the interlaminar degradation of longitudinal GFRP bars).

At a higher axial stiffness, however, G12N19-C4-100 exhibited an acceptable tendency compared to ST12N13-C4-100, as shown in Fig. 12(b). Up to 2.4% drift, both columns had similar E_{acc} , with ST12N13-C4-100 experiencing more loop opening, but G12N19-C4-100 attaining higher load. The longitudinal steel bars started buckling at 2.4% drift, resulting in ST12N10-C4-100 having a higher E_{acc} than G12N19-C4-100. With the ascending tendency of G12N19-C4-100 after 1.9% drift with continuous load increases until test termination at 10.1% drift and the descending tendency of ST12N10-C4-100 until loss of axial

capacity with a 50% reduction of the maximum lateral load, G12N19-C4-100 achieved more than 76% of the dissipated energy attained by ST12N10-C4-100 (refer to Fig. 12(b)), which is considered a satisfactory level of energy dissipation.

Figures 12(c) and (e) show that no clear effect of reinforcement configuration or spiral and tie spacing on the energy dissipation. A slight increase in the dissipated energy due to the increased ALR and longitudinal-reinforcement ratio was observed, as shown in Fig. 12(d) and (f), respectively.

Effect of axial load ratio (ALR)

Three ALR of $0.2f'_c A_g$, $0.3f'_c A_g$, and $0.4f'_c A_g$ were applied to G12N13-C4-100, G12N13-C4-100-30, and G12N13-C4-100-40, respectively, to study the effect of ALR. A limited increase in strength capacity was observed with increasing ALR, which coincides with the similarity of the estimated plan-sectional analysis flexural strength. Increasing the ALR was found to result in faster deterioration of the concrete core represented by the larger plastic hinge (refer to Fig. 9) and reduced the ductility capacity of the columns (refer to Table 4). Similar behavior was reported by Tavassoli et al. (2015) and Ali and El-Salakawy (2016) for laterally loaded circular and square GFRP-reinforced columns, respectively, where specimens with higher ALR showed faster deterioration with lower level of ductility capacity.

Effect of transverse reinforcement spacing

Increasing the transverse reinforcement ratio by decreasing the spacing significantly enhanced the ductility and yielded higher strength. Closer transverse reinforcement spacing resulted in better confinement of the concrete core and delayed the deterioration of either the longitudinal reinforcement or the concrete core. For instance, the drift for

Column G12N13-C4-80 was almost 60% higher than that of Column G12N13-C4-150. Reducing the spacing from 150 to 80 mm (5.9 to 3.15 in.) yielded a 23% increase in column strength capacity and delayed the drift corresponding to the interlaminar degradation of longitudinal bars from 3.8 to 6.7% (Table 3 and Fig. 5). Increasing the spacing from 80 mm to 100 mm (3.15 in. to 3.94 in.) (G12N13-C4-80 and G12N13-C4-100, respectively) resulted in a 13% reduction in column strength capacity with no significant difference in the overall behavior of the two columns (Table 3 and Fig. 5). This could indicate that the maximum spacing requirement by CSA S806-12 (maximum spacing for the specimens is controlled by $6d_b = 76.2$ mm [3 in.], where d_b is the longitudinal bar diameter) is restrictive.

COMPARISON TO DESIGN CODE

Clause 12.7 in CSA S806 (2012) gives complete detailing and limitations for designing lateral-resisting systems reinforced solely with FRP bars. This information was examined based on the outcomes of the GFRP-reinforced columns tested in this study.

The required area A_{sh} of the rectilinear spirals and cross ties provided in the tested GFRP-reinforced columns was calculated as follows

$$A_{sh} = 14s h_c \frac{f'_c}{f_{Fh}} \left(\frac{A_g}{A_c} - 1 \right) \frac{P}{P_o} \frac{\delta}{\sqrt{k_c}} \quad (6)$$

where $P/P_o \geq 0.2$ (applied axial load to the column's nominal unconfined axial-load), $(A_g/A_c - 1) \geq 0.3$ (A_g and A_c are the gross and core cross-sectional area of the column);

$k_c = 0.15 \sqrt{(h_c/s)(h_c/sl)}$, $f_{Fh} = 0.006 E_f$ or $\phi_f f_{fu}$, whichever is less; δ is the drift (0.025 and 0.04 for moderately ductile and ductile lateral-resisting systems, respectively); f'_c is the concrete compressive strength; h_c is the cross-sectional dimension of the column core; s is the spacing of transverse reinforcement, sl is the spacing of tie legs in the cross-sectional plane of the column; and E_f and f_{fu} are the modulus of elasticity and ultimate tensile strength of FRP transverse reinforcement, respectively.

All the tested GFRP-reinforced columns were designed using Eq. (6) to achieve either 2.5 or 4% drift except for two columns—G8N13-C1-100 and G12N13-C3-100—which were not provided with crossties (Table 1 and Fig. 1(c)). The drift that could be achieved by each column according to the transverse reinforcement actually provided was estimated using the back calculation of Eq. (6). Figure 13 shows the experimentally determined drift of the tested columns against the estimated drift. G8N13-C1-100 and G12N13-C3-100 clearly achieved higher drift than the estimated 1.5% and 1.4% drift, attaining up to 4.2% and 3.6% drift, respectively. Increasing the transverse reinforcement area by 33% (adding a single-leg crosstie to G8N13-C1-100) clearly enhanced the ductility capacity and ultimate drift of G8N13-C2-100 (refer to Table 4 and Fig. 5 and 13). Similarly, doubling the transverse reinforcement area of G12N13-C3-100 (adding a double-leg closed crosstie) enhanced not only G12N13-C4-100's ductility performance and ultimate drift but also its strength capacity. Generally, all the columns achieved much higher drift than the estimated values, confirming the effectiveness of using GFRP bars in lateral-resisting systems.

The design stress level in FRP transverse reinforcement f_{Fh} is limited to the least stress corresponding to a strain of 0.006, or the stress corresponding to the failure of the rectilinear spirals or crossties. The strain limitation (0.006) is usually the predominant parameter in defining stress level due to the high tensile strength of FRP. Figure 14 shows typical hysteretic response of strain in rectilinear spiral and crossties. The strain increased and fell back to zero in the early stages of loading. As the cover spalled, the plasticity of

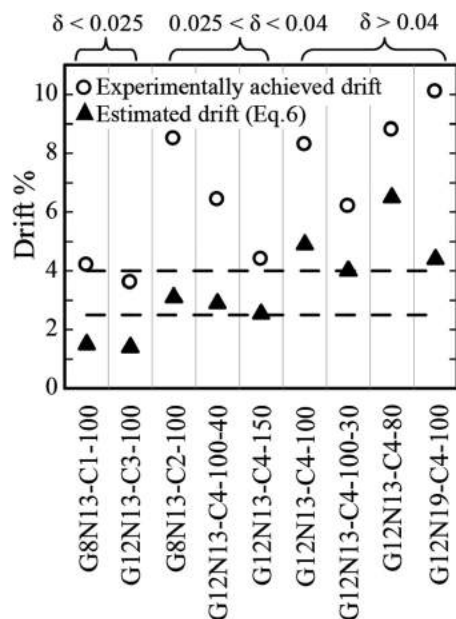


Fig. 13—Achieved versus estimated drift (Eq. (6)).

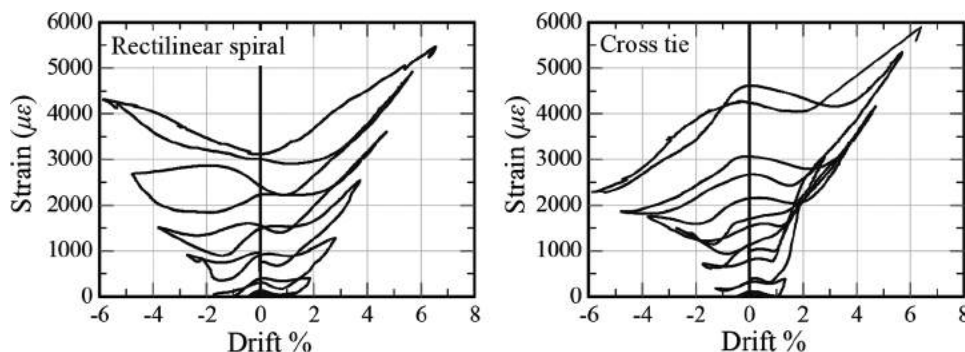


Fig. 14—Typical strain in rectilinear spirals and crossties (G12N13-C4-100).

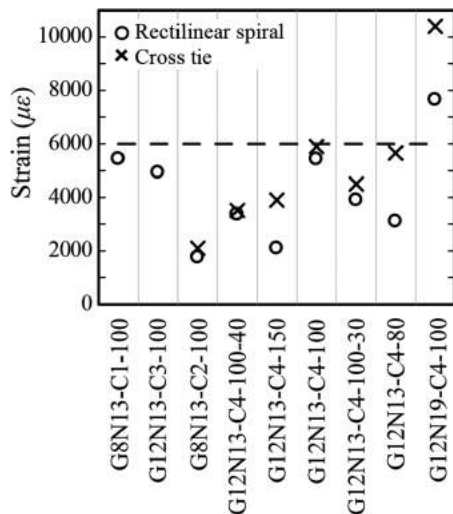


Fig. 15—Strain in rectilinear spirals and crossties in tested columns.

the concrete core initiated with noticeable strain values recorded at zero drift. Thereafter, the strain kept increasing with each cycle. Figure 15 shows the strain values in rectilinear spirals and crossties that were less than the strain limit of 0.006, confirming that the use of GFRP transverse reinforcement based on Eq. (6) effectively confined the concrete core in the post-peak stages. This agrees with the findings of Tobbi et al. (2014). Although Eq. (6) estimated similar A_{sh} for G12N13-C4-100 and G12N19-C4-100, the transverse strain was much higher in G12N19-C4-100, reaching 10,400 $\mu\epsilon$. This could be attributed to the greater longitudinal-bar diameter resulting in increased axial capacity and lateral resistance, as shown in Table 3 and Fig. 5. This, in return, induced higher transverse strains than those attained in G12N13-C4-100 (Fig. 15). Therefore, G12N19-C4-100 having higher transverse reinforcement area could keep the induced strain within the limit of 0.006. This observation addresses the importance of including the effect of longitudinal bars in calculating the required A_{sh} (Eq. (6)) either as bar diameter or area as well as the number of bars. Moreover, this point confirms the capability of using GFRP bars to carry axial load combined with lateral load.

CONCLUSIONS

This paper presents a test program aimed at studying the behavior of 11 steel- and GFRP-reinforced columns under simulated earthquake loading. Based on the analysis of the experimental results, the following conclusions were reached:

1. The hysteresis loops of the GFRP-reinforced columns reflected stable cyclic behavior with no or limited strength degradation, less than that experienced by the steel-reinforced columns.

2. The ability of the GFRP-reinforced columns to achieve higher Δ_u than the steel-reinforced columns compensates for the high values of Δ_e of the GFRP-reinforced columns compared to Δ_y of the steel ones. This allows the GFRP-reinforced columns to achieve a deformability capacity comparable to steel-reinforced columns.

3. Increasing the axial load level negatively affected the ductility capacity of the GFRP-reinforced columns with negligible lateral strength gain.

4. The elastic behavior of the GFRP rectilinear spirals and crossties enhanced the confinement of the concrete core, delaying crushing. Yielding in the transverse steel reinforcement resulted in early degradation of the core concrete.

5. The achieved drifts for the GFRP-reinforced columns were in a range between 50 and 180% more than the estimated values, clarifying the conservative limits of Eq. (6).

6. The longitudinal bar size should be included in calculating the required transverse reinforcement area for GFRP-reinforced columns, requiring a larger transverse-reinforcement area to comply with the strain limitation of Eq. (6).

Therefore, because the GFRP-reinforced columns attained good strength and deformation capacity, GFRP reinforcement could be used in lateral resisting systems, although further research is needed to implement adequate design guidelines and recommendations for such structural elements.

AUTHOR BIOS

Mohammed G. Elshamandy is a Doctoral Candidate in the Department of Civil Engineering, University of Sherbrooke, Sherbrooke, QC, Canada. He received his BSc and MSc from Assiut University, Assiut, Egypt. His research interests include testing of concrete structures reinforced with fiber-reinforced polymers.

Ahmed Sabry Farghaly is a Postdoctoral Fellow in the Department of Civil Engineering at the University of Sherbrooke. His research interests include full-scale testing, nonlinear analysis, and design of concrete structures reinforced with fiber-reinforced polymers.

Brahim Benmokrane, FACI, is Professor of civil engineering and NSERC Research Chair in FRP Reinforcement for Concrete Infrastructure and Tier-1 Canada Research Chair in Advanced Composite Materials for Civil Structures in the Department of Civil Engineering at the University of Sherbrooke. He is a member of ACI Committee 440, Fiber-Reinforced Polymer Reinforcement.

ACKNOWLEDGMENTS

This experimental study was conducted with funding from the Tier-1 Canada Research Chair in Advanced Composite Materials for Civil Structures (CRC Research Program). The assistance of the technical staff of the new Canadian Foundation for Innovation (CFI) structural lab at the University of Sherbrooke's Department of Civil Engineering is also acknowledged.

REFERENCES

- ACI Committee 318, 2014, "Building Code Requirements for Structural Concrete (ACI 318-14) and Commentary (ACI 318R-14)," American Concrete Institute, Farmington Hills, MI, 519 pp.
- ACI Committee 440, 2004, "Guide Test Methods for Fiber-Reinforced Polymers (FRPs) for Reinforcing or Strengthening Concrete Structures (ACI 440.3R-04)," American Concrete Institute, Farmington Hills, MI, 40 pp.
- ACI Committee 440, 2007, "Report on Fiber-Reinforced Polymer (FRP) Reinforcement Concrete Structures (ACI 440R-07)," American Concrete Institute, Farmington Hills, MI, 100 pp.
- ACI Committee 440, 2015, "Guide for the Design and Construction of Concrete Reinforced with FRP Bars (ACI 440.1R-15)," American Concrete Institute, Farmington Hills, MI, 44 pp.
- Afifi, M.; Mohamed, H.; and Benmokrane, B., 2014, "Axial Capacity of Circular Concrete Columns Reinforced with GFRP Bars and Spirals," *Journal of Composites for Construction*, ASCE, V. 18, No. 1, p. 04013017 doi: 10.1061/(ASCE)CC.1943-5614.0000438
- Ali, M. A.; and El-Salakawy E., 2016, "Seismic Performance of GFRP-Reinforced Concrete Rectangular Columns," *Journal of Composites for Construction*, ASCE, V. 20, N. 3, p. 04015074. doi: 10.1061/(ASCE)CC.1943-5614.0000637

- Alsayed, S. H.; Al-Salloum, Y. A.; Almusallam, T. H.; and Amjad, M. A., 1999, "Concrete Columns Reinforced by GFRP Rods," *Fourth International Symposium on Fiber-Reinforced Polymer Reinforcement for Reinforced Concrete Structures*, SP-188, C. W. Dolan, S. H. Rizkalla, and A. Nanni, eds., American Concrete Institute, Farmington Hills, MI, pp. 103-112.
- ASTM D7205-11, 2011, "Standard Test Methods for Tensile Properties of Fiber-Reinforced Polymer Matrix Composite Bars," ASTM International, West Conshohocken, PA, 13 pp.
- Bakis, C. E.; Bank, L. C.; Brown, V. L.; Cosenza, E.; Davalos, J. F.; Lesko, J. J.; Machida, A.; Rizkalla, S. H.; and Triantafillou, T. C., 2002, "Fiber-Reinforced Polymer Composites for Construction—State-of-the-Art Review," *Journal of Composites for Construction*, ASCE, V. 6, No. 2, pp. 73-87. doi: 10.1061/(ASCE)1090-0268(2002)6:2(73)
- CAN/CSA A23.3-14, 2014, "Design of Concrete Structures Standard," Canadian Standards Association, Mississauga, ON, Canada, 2004, 240 pp.
- CAN/CSA S6-14, 2014, "Canadian Highway Bridge Design Code," Canadian Standards Association, Mississauga, ON, Canada, 1078 pp.
- CAN/CSA S806-12, 2012, "Design and Construction of Building Components with Fiber-Reinforced Polymers," Canadian Standards Association, Mississauga, ON, Canada, 208 pp.
- CAN/CSA S807-15, 2015, "Specification for Fibre Reinforced Polymers," Canadian Standards Association, Mississauga, ON, Canada, 44 pp.
- Choo, C. C.; Harik, I. E.; and Gesund, H., 2006, "Strength of Rectangular Concrete Columns Reinforced with Fiber-Reinforced Polymer Bars," *ACI Structural Journal*, V. 103, No. 3, May-June, pp. 452-459.
- De Luca, A.; Matta, F.; and Nanni, A., 2010, "Behavior of Full-Scale Glass Fiber-Reinforced Polymer Reinforced Concrete Columns under Axial Load," *ACI Structural Journal*, V. 107, No. 5, Sept.-Oct., pp. 589-596.
- El-Salakawy, E.; Benmokrane, B.; El-Ragaby, A.; and Nadeau, D., 2005, "Field Investigation on the First Bridge Deck Slab Reinforced with Glass FRP Bars Constructed in Canada," *Journal of Composites for Construction*, ASCE, V. 9, No. 6, pp. 470-479. doi: 10.1061/(ASCE)1090-0268(2005)9:6(470)
- Fédération Internationale du Béton (*fib*) 2007, "FRP Reinforcement in RC Structures," Task Group 9.3, Lausanne, Switzerland, 147 pp.
- Jaeger, L. G.; Tadros, G.; and Mufti, A. A., 1995, "Balanced Section, Ductility and Deformability in Concrete with FRP Reinforcement." *Technical Report No. 2-1995*, Nova Scotia CAD/CAM Centre, Technical University of Nova Scotia, Halifax, NS, Canada.
- Kassem, C.; Farghaly, A. S.; and Benmokrane, B., 2011, "Evaluation of Flexural Behavior and Serviceability Performance of Concrete Beams Reinforced with FRP Bars," *Journal of Composites for Construction*, ASCE, V. 15, No. 5, pp. 682-695. doi: 10.1061/(ASCE)CC.1943-5614.0000216
- Mady, M.; Elragaby, A.; and Elsalakawy, E., 2011, "Seismic Behavior of Beam-Column Joints Reinforced with GFRP Bars and Stirrups," *Journal of Composites for Construction*, ASCE, V. 15, No. 6, pp. 875-886. doi: 10.1061/(ASCE)CC.1943-5614.0000220
- Mohamed, N.; Farghaly, A. S.; and Benmokrane, B., 2015, "Aspects of Deformability of Concrete Shear Walls Reinforced with Glass Fiber-Reinforced Bars," *Journal of Composites for Construction*, ASCE, V. 19, No. 5, p. 06014001 doi: 10.1061/(ASCE)CC.1943-5614.0000529
- Mohamed, N.; Farghaly, A. S.; Benmokrane, B.; and Neale, K. W., 2014, "Experimental Investigation of Concrete Shear Walls Reinforced with Glass-Fiber-Reinforced Bars under Lateral Cyclic Loading," *Journal of Composites for Construction*, ASCE, V. 18, No. 3, p. A4014001 doi: 10.1061/(ASCE)CC.1943-5614.0000393
- National Research Council of Canada, NRC, 2010, "Canadian Commission on Building and Fire Codes," National Building Code of Canada (NBC), Ottawa, ON, Canada, 1167 pp.
- Sharbatdar, M. K., and Saatcioglu, M., 2009, "Seismic Design of FRP Reinforced Concrete Structures," *Asian Journal of Applied Sciences*, V. 2, No. 3, pp. 211-222. doi: 10.3923/ajaps.2009.211.222
- Sheikh, S. A., and Houry, S. S., 1993, "Confined Concrete Columns with Stubs," *ACI Structural Journal*, V. 90, No. 4, July-Aug., pp. 414-431.
- Tavassoli, A.; Liu, J.; and Sheikh, S., 2015, "Glass Fiber-Reinforced Polymer-Reinforced Circular Columns under Simulated Seismic Loads," *ACI Structural Journal*, V. 112, No. 1, Jan.-Feb., pp. 103-114.
- Tobbi, H.; Farghaly, A. S.; and Benmokrane, B., 2012, "Concrete Columns Reinforced Longitudinally and Transversally with Glass Fiber-Reinforced Polymers Bars," *ACI Structural Journal*, V. 109, No. 4, July-Aug., pp. 551-558.
- Tobbi, H.; Farghaly, A. S.; and Benmokrane, B., 2014, "Strength Model for Concrete Columns Reinforced with Fiber-Reinforced Polymer Bars and Ties," *ACI Structural Journal*, V. 111, No. 4, July-Aug., pp. 789-798.
- Zadeh, H. J., and Nanni, A., 2013, "Design of RC Columns Using Glass FRP Reinforcement," *Journal of Composites for Construction*, V. 17, No. 3, June, pp. 294-304.

CALL FOR ACTION

ACI Invites You To...

**Share your
expertise**

Do you have EXPERTISE in any of these areas?

- BIM
- Chimneys
- Circular Concrete Structures Prestressed by Wrapping with Wire and Strand
- Circular Concrete Structures Prestressed with Circumferential Tendons
- Concrete Properties
- Demolition
- Deterioration of Concrete in Hydraulic Structures
- Electronic Data Exchange
- Insulating Concrete Forms, Design, and Construction
- Nuclear Reactors, Concrete Components
- Pedestal Water Towers
- Pipe, Cast-in-Place
- Strengthening of Concrete Members
- Sustainability

**Become a
Reviewer for the
ACI Journals**

**Then become a REVIEWER for the
ACI Structural Journal or the *ACI Materials Journal*.**

How to become a Reviewer:

1. Go to: <http://mc.manuscriptcentral.com/aci>;
2. Click on "Create Account" in the upper right-hand corner; and
3. Enter your E-mail/Name, Address, User ID and Password, and Area(s) of Expertise.

**Update your
Manuscript
Central user
account
information**

**Did you know that the database for MANUSCRIPT
CENTRAL, our manuscript submission program,
is separate from the ACI membership database?**

How to update your user account:

1. Go to <http://mc.manuscriptcentral.com/aci>;
2. Log in with your current User ID & Password; and
3. Update your E-mail/Name, Address, User ID and Password, and Area(s) of Expertise.

QUESTIONS?

E-mail any questions to Journals.Manuscripts@concrete.org.



American Concrete Institute

Always advancing